ACS APPLIED MATERIALS & INTERFACES

Research Article

www.acsami.org

Doping Effect of Organosulfonic Acid in Poly(3-hexylthiophene) Films for Organic Field-Effect Transistors

Sungho Nam,[†] Joonhyeon Kim,[†] Hyena Lee,[†] Hwajeong Kim,*[,†,‡] Chang-Sik Ha,*[,†,§] and Youngkyoo Kim*[,†,‡]

[†]Organic Nanoelectronics Laboratory, Department of Chemical Engineering, and [‡]Research Institute of Advanced Energy Technology, Kyungpook National University, Daegu 702-701, Republic of Korea

[§]Department of Polymer Science and Engineering, Pusan National University, Busan 609-735, Republic of Korea

Supporting Information

ABSTRACT: We attempted to dope poly(3-hexylthiophene) (P3HT) with 2-ethylbenzenesulfonic acid (EBSA), which has good solubility in organic solvents, in order to improve the performance of organic field effect transistors (OFET). The EBSA doping ratio was varied up to 1.0 wt % because the semiconducting property of P3HT could be lost by higher level doping. The doping reaction was confirmed by the emerged absorption peak at the wavelength of ~970 nm and the shifted S2p peak (X-ray photoelectron spectroscopy), while the ionization potential and nanostructure of P3HT films was slightly affected by the EBSA doping. Interestingly, the EBSA doping delivered significantly improved hole mobility because of the greatly enhanced drain current of OFETs by the presence of the permanently charged parts in the P3HT chains. The hole mobility after the EBSA doping was increased by the factor of 55−86 times depending on the regioregularity at the expense of low on/off ratio in the case of unoptimized devices, while the optimized devices showed ~10 times increased hole mobility by the 1.0 wt % EBSA doping with the greatly improved on/off ratio even though the source and drain electrodes were made using relatively cheaper silver instead of gold.

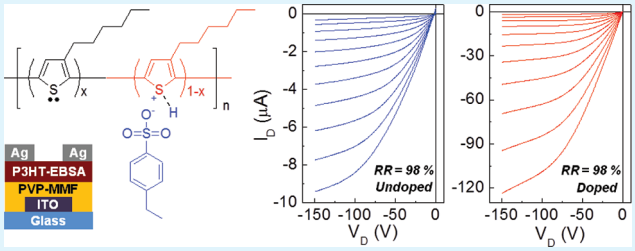

KEYWORDS: *organic field-effect transistors, P3HT, organosulfonic acid, regioregularity, silver*

INTRODUCTION

For the last two decades, organic field-effect transistors (OFET) have been extensively studied by employing organic semiconductors including either small molecules or polymers.[1−5] Because of the limited availability of suitable electrode materials for minimizing the charge injection energy barrier from the source/drain electrodes to organic semiconductor layer or vice versa, the p-type OFETs have been relatively widely studied compared to the n-type OFETs.[3,4] To date, the highest (reproducible) hole mobility of small molecular p-type OFETs reached ~1.5 $cm^2/V{\cdot}s$ by using high purity pentacene derivatives,[6] although extremely high mobility (~15 $cm^2/V{\cdot}s$) has been reported for the OFETs with organic single crystals.[7] In the case of polymer OFETs, polythiophene derivatives (mostly, regioregular poly(3-hexylthiophene) (P3HT)) exhibited the record-high hole mobility of ~3.3 $cm^2/(V\ s)$ due to their self-organizing tendency leading to high crystallinity.[8,9] Considering the best mobility values achieved so far, it is concluded that the better the crystallinity, the higher the charge (hole) transportability in OFET structures. In particular, the high crystallinity (leading to high charge mobility) of P3HTs was found to help improve the performance of polymer/fullerene solar cells.[10]

As an alternative approach to improve the hole mobility of p-type organic semiconductors, two different doping techniques have been introduced. One approach is electrochemical doping of an ammonium salt (tetraethylammomium perchlorate) into P3HT films,[11] another is doping (mixing) of an electron acceptor (2,3,5,6-tetrafluoro-7,7,8,8-tetracyanoquinodimethane (F_4-TCNQ)) into organic semiconductor films.[12−14] However, these two approaches have a fundamental drawback in terms of doping control and solution processability because the solubility of ammonium salt and F_4-TCNQ is extremely poor in organic solvents that dissolve most of organic semiconductors. The poor solubility of those doping materials can give rise to an unstable morphology of resulting organic semiconductor films leading to a catastrophic degradation of OFETs upon operation. Recently, we made a progress to improve the charge carrier (electron) mobility and solar cell performances by using an n-type polymer that is doped with an organosulfonic acid in solutions.

Hence, in this work, we attempted to dope organic semiconductors (P3HT) with an organosulfonic acid (4-

Received: November 4, 2011
Accepted: January 30, 2012
Published: January 30, 2012

ethylbenzenesulfonic acid (EBSA)) in an organic solvent (chlorobenzene) and fabricated OFETs with the EBSA-doped P3HT (hereafter, P3HT-EBSA) films. To understand the effect of EBSA doping according to the regioregularity, we briefly investigated the characteristics of OFETs with the P3HT films (three different regioregularities). In addition, taking into account the commercial aspect of OFETs, a silver (Ag) metal was employed as a top contact electrode (source and drain electrodes) instead of gold (Au) even though there is a demerit for its slightly larger injection barrier compared to the Au electrode.[15] Results showed that the hole mobility of the optimized OFETs with the 1.0 wt % EBSA-doped P3HT films was improved by ca. 10-fold in the presence of high on/off ratio even though silver source and drain electrodes were used instead of expensive gold.

EXPERIMENTAL SECTION

Materials. P3HT polymers were supplied from Rieke Metals and used without further purification. The regioregularity of P3HT polymers was 92% (weight-average molecular weight (M_w) = 5.9 × 10^4 and polydispersity index (PDI) = 2.32), 95% (M_w = 6.0 × 10^4 and PDI = 2.0), and 98% (M_w = 2.0 × 10^4 and PDI = 2.0). EBSA (dopant), poly(vinylphenol) (PVP), methylated poly(melamine-co-formaldehyde) (MMF), chlorobenzene (solvent for P3HT and EBSA), propylene glycol monomethyl ether acetate (PGMEA) (solvent for PVP and MMF), and Ag (purity =99.99%) wire were purchased from Sigma-Aldrich. The number-average molecular weight of MMF was ca. 432 and was dissolved in 1-butanol (84 wt %, Sigma-Aldrich).

Solutions and Doping Process. The P3HT polymers were dissolved in chlorobenzene at a solid concentration of 20 mg/mL. To the P3HT solutions were added the EBSA molecules, and the solutions were vigorously stirred to achieve a clear solution. The doping ratio of EBSA to P3HT was varied up to 1.0 wt %. These solutions were continuously stirred to complete doping process at 60 °C for ~2 days. To make the PVP-MMF films (gate insulator), PVP (100 mg) and MMF (125 mg) were mixed using the PGMEA solvent (1 mL).

Film and Device Fabrication. The pristine P3HT and P3HT-EBSA films were spin-coated on quartz substrates for optical absorption and photoluminescence (PL) measurements, while they were spun on indium tin-oxide (ITO)-coated glass substrates for the measurement of photoelectron yield spectroscopy (PEYS), ultraviolet photoelectron spectroscopy (UPS) and X-ray photoelectron spectroscopy (XPS). Prior to fabricating OFET devices, the ITO-glass substrates were cleaned using acetone and isopropyl alcohol. On top of the cleaned ITO-glass substrates, the mixture solutions of PVP and MMF were spin-coated and dried at 120 °C for 10 min. These precursor mixture films were thermally cured at 250 °C for 60 min to have insoluble PVP-MMF gate insulator films (thickness =7 00 nm). Next, the pristine P3HT and P3HT-EBSA films (channel layer, thickness = 50 nm) were spin-coated on the PVP-MMF layers that were coated on the ITO-glass substrates. After drying the channel layers at 50 °C for 15 min, the samples were loaded into vacuum chamber that is installed inside a nitrogen-filled glovebox. Then the Ag electrodes were deposited on the channel layers of the samples through a metal shadow mask, which defines a channel length of 70 μm and a channel width of 3 mm. To investigate the influence of thermal annealing of film samples and devices, parts of samples were thermally annealed at 120 °C for 30 min.

Measurements. The optical absorption spectra of the pristine P3HT and P3HT-EBSA films coated on quartz substrates were measured using a UV−visible spectrometer (optizen 2120UV, Mecasys), while their PL spectra were measured by exciting the samples at 525 nm using a PL spectrometer (FP-6500, JASCO). The XPS spectra of the pristine P3HT and P3HT-EBSA films coated on the ITO-glass substrates were measured using a XPS measurement system (ESCALAB 250, VG Scientifics). The ionization potential or highest occupied molecular orbital (HOMO) energy of the pristine P3HT and P3HT-EBSA films coated on the ITO-glass substrates were measured using a PE yield spectrometer (PEYS, AC2, Riken-Keiki) and an UPS system (AXIS, Kratos Inc.). The nanostructure of the pristine P3HT and P3HT-EBSA layers (films), which were coated on the PVP-MMF layers of the samples, were measured using a synchrotron radiation grazing angle incidence X-ray diffraction (GIXD) system (Pohang Accelerator Laboratory, South Korea) and high resolution transmission electron microscope (HRTEM, Tecnai G2 F20 S-TWIN, PHILIPS). The surface morphology of the pristine P3HT and P3HT-EBSA layers, which were coated on the PVP-MMF layers of the samples, were measured using an atomic force microscope (AFM, Nanoscope IIIa, Digital Instruments) and an Auger electron microscope (AEM, PHI 700, ULVAC-PHI).

RESULTS AND DISCUSSION

Doping Reaction and Characterization. As shown in Figure 1, the doping reaction of P3HT was carried out with two

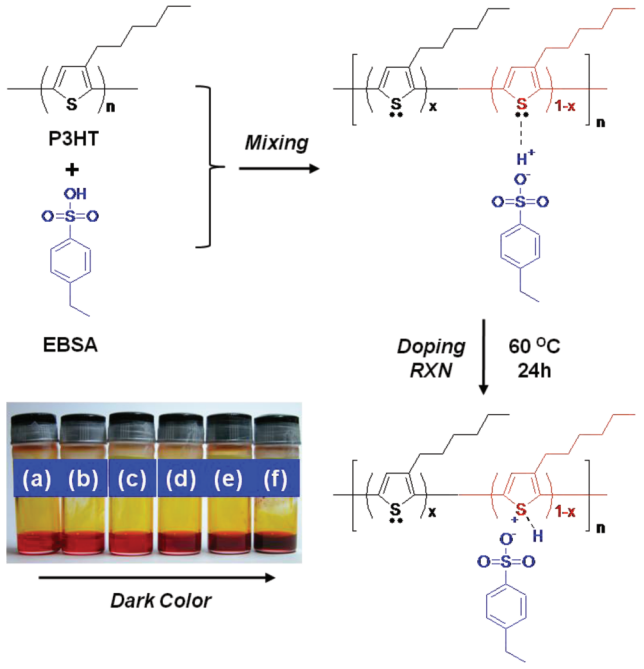

Figure 1. Schematic illustration for the doping reaction of P3HTwith EBSA in chlorobenzene. Photograph: EBSA (wt %) = (a) 0, (b) 0.1, (c) 0.3, (d) 0.5, (e) 0.7, and (f) 1.0.

steps. At the mixing stage the solutions were vigorously stirred at room temperature in order to induce a close interaction between P3HT and EBSA molecules (more precisely, to make Coulombic interaction between the lone pair electrons in the sulfur atoms of P3HT and the sulfonic acid groups of EBSA). After confirming that the solutions become optically clear without any insoluble components, the solutions were heated up to 60 °C and stirred for 24 h to complete the doping reaction. As seen from the photograph (left bottom side in Figure 1), the solution color became darker as the doping ratio increased. This noticeable change of solution color with only small variation of EBSA content indicates that the doping reaction indeed occurred in the present condition (we note that the EBSA itself showed a slight yellowish color in solution but this did not affect the color change in the mixture (P3HT + EBSA) solutions because the maximum EBSA content was only 1.0 wt %.

To characterize the doped states, the optical absorption and PL spectra of the pristine and P3HT-EBSA films were

measured. As shown in Figure 2a, very little change in the absorption spectra was observed after doping in the range of

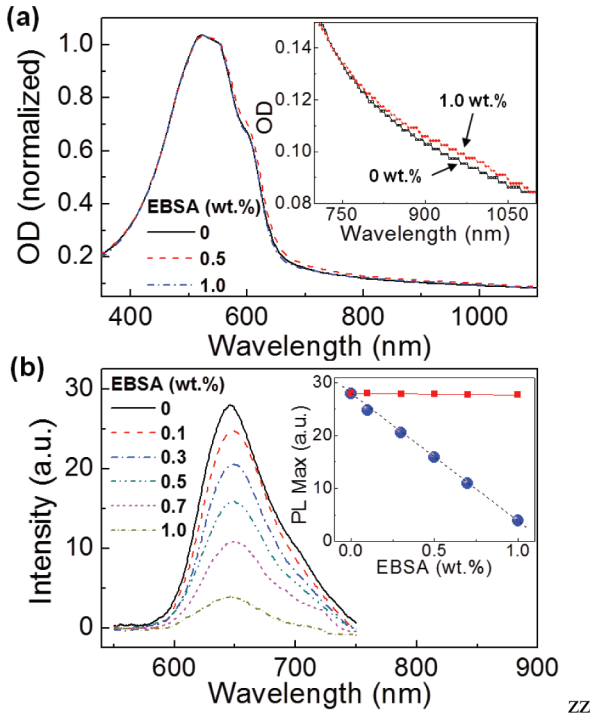

Figure 2. (a) Optical absorption and (b) PL spectra of pristine P3HT and P3HT-EBSA films. The inset in a′ shows the enlarged absorption spectra in the range of longer wavelength regions for the pristine P3HT film and the P3HT-EBSA (1.0 wt %) film. The inset in b′ shows the PL intensity change as a function of the EBSA content (filled circles), whereas the filled squares (red) denote the calculated PL intensity using a simple additive rule.

longer wavelengths (>600 nm). This slight change can be attributed to the considerably small amount (maximum 1.0 wt %) of EBSA compared to the P3HT content. The marginally higher intensity (>600 nm) of the P3HT-EBSA film for 0.5 wt % compared to 1.0 wt % doping might be attributed to the role of EBSA molecules which affects the P3HT crystallization behavior at a particular EBSA concentration. Comparing between the pristine P3HT film and the P3HT-EBSA (1.0 wt %) film (inset in Figure 2a), we find that the P3HT-EBSA (1.0 wt %) film showed new peak at around 970 nm (~1.3 eV) which can be ascribed to the EBSA-doped thiophene units in the P3HT chains (see also Figure S1 in the Supporting Information for the optical absorption spectra of highly doped P3HT-EBSA films). This doping effect was pronouncedly observed from the PL spectra in Figure 2b. As the doping ratio increased, the maximum PL intensity was gradually decreased in the presence of (relative) growth of new peak at around 700−730 nm. This PL quenching phenomenon evidences that there exist positively charged (doped) units in the P3HT chains which act as a trap to quench the excitons generated in the films. Here it is noteworthy that the degree of PL decay (ca. 10 times reduction from the pristine film by 1.0 wt % EBSA doping) overwhelms the dilution effect (only 1.0 wt % maximum) of EBSA (leading to the reduction in the number of P3HT chains in the film). In addition, considering the nature of P3HT chain stacking, it is expected that the PL intensity should be increased if any dilution effect without exciton quenching.[16,17]

To further characterize the doping status, the XPS spectra of the pristine P3HT and P3HT-EBSA films were measured as shown in Figure 3. First, the C1s peaks were investigated but

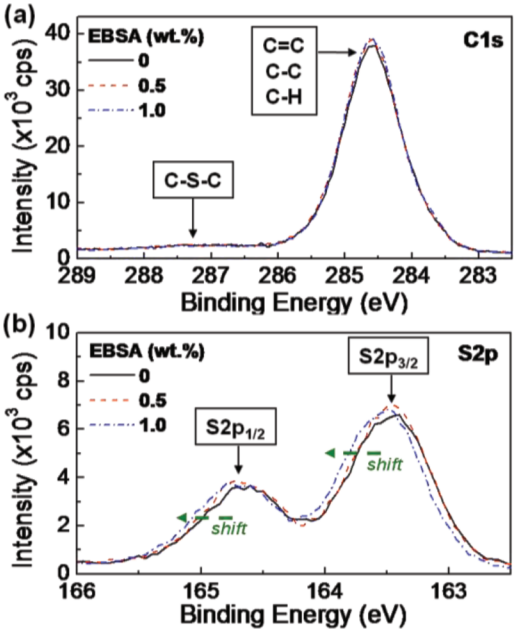

Figure 3. XPS spectra of pristine P3HT and P3HT-EBSA films: (a) C1s spectra, (b) S2p spectra.

no particular change (peak shift) was found though the peak at around 284.6 eV was marginally increased after doping (see Figure 3a). This result implies that the environment of carbon atoms in the P3HT chains was not affected by the EBSA doping. In contrast, a gradual shift in the S2p peaks was measured with the EBSA content (see Figure 3b), indicating that the environment of sulfur atoms in the P3HT chains was changed by the EBSA doping. However, the extent of the S2p peak shift was not so large because the maximum EBSA doping ratio was only 1.0 wt %.[18−20]

As a final step for the EBSA doping characterization, the ionization potential of the pristine P3HT and P3HT-EBSA films was measured. As shown in Figure 4a, the PE yield spectra (PEYS) of samples seem to be almost similar each other, but a close look at the take-up part at around 4.5−4.8 eV discloses that the photon energy for the PE yield onset became slightly lowered as the EBSA doping ratio increased (see inset figure in Figure 4a). To confirm this shift, we tried the UPS measurement of the pristine and P3HT-EBSA films. As shown in Figure 4b, the spectral shape of all samples seems to be almost similar as observed from the PEYS measurements. However, magnifying the low binding energy region of the UPS spectra (related to the upper part of HOMO level), we found that the peak was shifted toward the lower binding energy region as the EBSA doping ratio increased. This UPS result is in good agreement with the PEYS result, which confirms that the doping of small amount of EBSA molecules indeed changed the electronic structure of P3HT films, even though the change was very small. Taking into account the similar low level doping of conventional inorganic semiconductors which results in huge change of their electrical properties, however, the present 1.0 wt

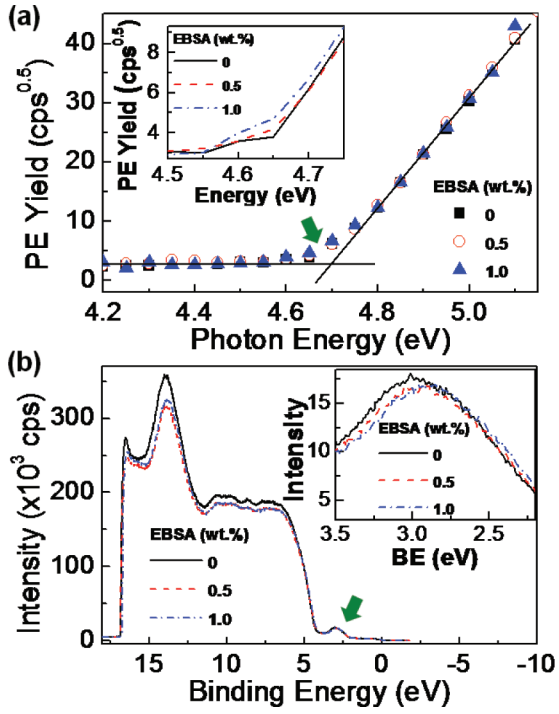

Figure 4. (a) PEYS and (b) UPS spectra of pristine P3HT and P3HT-EBSA films: Green arrows denote the enlarging part for each inset figure. Note that the PEYS spectra were measured under atmospheric condition, whereas the UPS spectra were measured at ultrahigh vacuum (1×10^{-10} to 1×10^{-8} Torr).

% EBSA doping is expected to be sufficient for modifying the semiconducting characteristics of the pristine P3HT film.

Energy Band Diagram and Mechanism. On the basis of the above characterization results, we can build an energy band diagram of P3HT in the presence of (EBSA) doped states. As shown in Figure 5a, the HOMO energy level was obtained as

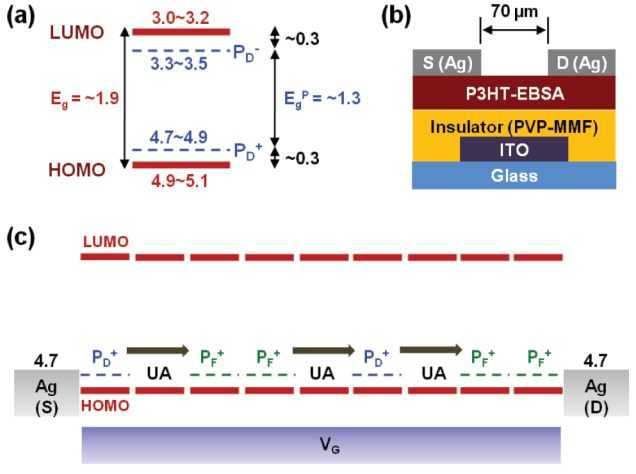

Figure 5. (a) Energy band diagram of P3HT-EBSA, (b) schematic illustration of the OFET with the P3HT-EBSA channel layer, and (c) illustration of charge transport through the P3HT-EBSA channel layer upon applying the gate voltage. E_g, Eg^P, P_D^+, P_D^-, P_F^+, P_F^-, S, D, and UA denote the band gap energy of P3HT, the band gap energy of doped state (P3HT-EBSA), the positive polaron level by doping, the negative polaron level by doping, the positive polaron level by field-effect, the negative polaron level by field effect, the source electrode, the drain electrode, and the unaffected part by field effect, respectively.

4.9−5.1 eV from the PEYS result after calibration,[15,21] while the optical band gap ($E_g \approx 1.9$ eV) was calculated from the onset point of the absorption spectrum of P3HT (see Figure 2a). Next, the position of positive (P_D^+) and negative (P_D^-) polarons, which were generated by the EBSA doping, was determined by the polaron band gap energy ($E_g^P \approx 1.3$ eV from the absorption peak at ~970 nm in Figure 2a inset). Here, if we fabricate OFETs as depicted in Figure 5b, the charge (hole) transport can be occurred as illustrated in Figure 5c. In detail, although the (field-induced) positive polarons (P_F^+) are generated at the interface region of P3HT on the PVP-MMF layer by applying the gate voltage (V_G), the yield of P_F^+ generation is expected to be imperfect leading to the presence of insufficient charge transport pathways in the P3HT film. Therefore, this neutral P3HT part that is unaffected by the applied gate voltage (see "UA" in Figure 5c) can be one of limiting factors for high charge mobility. Here, if the permanently charged parts (P_D^+) are present even in a small portion, the charge transport can be more active by compensating the drawback of the "UA" parts at least. In addition, the energy level of the P_D^+ part is much closer to the work function of source and drain electrodes (Ag) so that the demerit of Ag electrodes compared to the Au electrodes can be complemented. However, the disadvantage of the presence of the permanently charged parts (P_D^+) could be relatively higher current flow at V_G = 0 V, even though this problem can be resolved by setting the gate voltage to negative voltages (V_G < 0 V).

OFET Characteristics. The suggested mechanism in Figure 5c is supported from the characteristic trends of OFETs. As shown in Figure 6a (top), the output curve of the OFET with

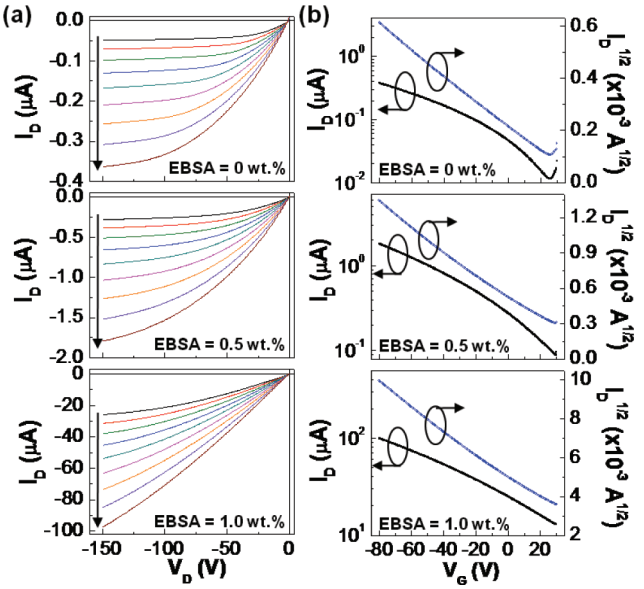

Figure 6. (a) Output and (b) transfer curves of OFETs with the pristine P3HT layer or the P3HT-EBSA layer: The gate voltage (V_G) increased negatively from 0 to −80 V by 10 V gap in the direction of the arrows in a′.

the pristine P3HT layer was gradually increased as the gate voltage increased up to −80 V. As typical for conventional P3HT OFETs, the saturation behavior was also observed in the present devices and the maximum output current was ca. −0.36 μA at V_G = −80 V and V_D = −150 V. When the P3HT-EBSA

dx.doi.org/10.1021/am300141m | ACS Appl. Mater. Interfaces 2012, 4, 1281−1288

(0.5 wt %) layer was used as a channel layer (Figure 6a middle), the saturation behavior of output curves became slightly weaker but the maximum output current reached ca. −1.8 μA at V_G = −80 V and V_D = −150 V. This is about 5 times improved result compared to the result of the OFET with the undoped (pristine) P3HT layer. In the case of 1.0 wt % doping (Figure 6a bottom), the maximum output current became ca. −100 μA at V_G = −80 V and V_D = −150 V, which is ∼277 times improved result from the value of the OFET with the pristine P3HT layer (see Figure S2 in the Supporting Information for the whole doping ratios). However, we note that the output current at V_G = 0 V and V_D = −150 V became also higher after doping, which can be assumed partly to the existence of permanent charges in the P3HT chains by the EBSA doping, as expected in the discussion in Figure 5c. This negative effect can be considerably resolved by programming the off-state to the positive gate voltage (for example, V_G = −80 V for on-state and V_G = +30 V for off-state). As shown in the transfer curves (Figure 6b), the threshold voltage (V_{TH}) was around −25 V even for the OFET with the pristine P3HT layer (Figure 6b top), which indicates the poor function of the (imperfect) gate dielectric layer (PVP-MMF) that was (slightly) negatively charged owing to the polar (unreacted) remnant hydroxyl groups as well as electron-rich ether linkages leading to generating a marginal amount of positive charges in the channel layer. This high V_{TH} value (to the positive voltage direction) is similarly applied for the OFETs with the P3HT-EBSA layers and the V_{TH} value became much higher as the EBSA doping ratio increased (see Figure 6b middle and bottom and Figure S2 in the Supporting Information). After thermal annealing of devices at 120 °C for 30 min, the output current was slightly decreased for all OFETs but the trend with the EBSA doping ratio was similar to that for the unannealed devices (see Figures S3 and S4 in the Supporting Information).

From the data in Figure 6b, the hole mobility of devices was obtained as shown in Figure 7a (top). As the doping ratio increased, the hole mobility tended to slowly increase initially and showed quick increase up to ∼3 × 10^{-2} $cm^2/(V\,s)$ at the doping ratio of 0.7 and 1.0 wt %. This increment is as high as 200 times from the hole mobility of the OFET with the pristine P3HT layer. Here we note that the actually measured dielectric constant (PVP-MMF = 3.5) was used to calculate the hole mobility. To understand the influence of conductivity change (induced by the EBSA doping) on the mobility, the resistance from I_D−V_D curves was measured for the selected samples. As shown in Figure 7a (bottom), the resistance was decreased with increasing the EBSA ratio, which reflects the increased conductivity by the generation of permanent charges (EBSA-doped thiophene parts). Finally we can see the inverse proportion of hole mobility with respect to the resistance in Figure 7b but further investigation is required for the mobility-conductivity correlation in the present doping systems.

Nanostructure and Morphology. Next, we investigated the nanostructure change in the P3HT layers after the EBSA doping. As shown in Figure 8a (2D GIXD images),[9,10,15,22,23] no particular crystal diffraction pattern was measured for the PVP-MMF layer coated on the ITO-glass substrate though a broad amorphous halo was observed in the wide range (see also the 1D GIXD diffractogram in Figure 8b). However, a distinct diffraction peak was clearly measured for the P3HT layer on the PVP-MMF-coated samples. However, no particular difference after the EBSA doping was seen from the 2D images, except the broad and diffused amorphous parts in the wider angle range.

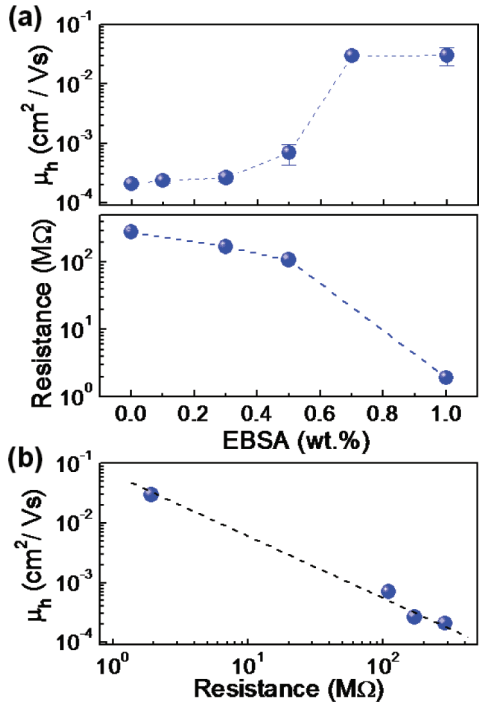

Figure 7. (a) Hole mobility (μ_h) and resistance as a function of EBSA doping ratio. (b) Relationship between the hole mobility and the resistance from a′.

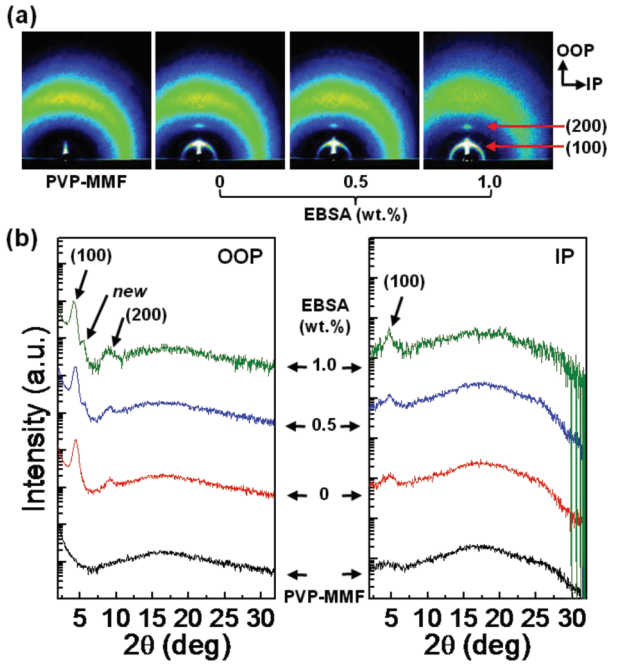

Figure 8. (a) 2D GIXD images of the PVP-MMF layer coated on the ITO-glass substrate and the pristine P3HT layer or the P3HT-EBSA layer coated on the PVP-MMF-coated samples. (b) 1D GIXD profiles extracted from the 2D images in a′. Note that all samples were prepared identically as used for the fabrication of OFETs.

From the 1D profiles extracted from the 2D images, we found that a new diffraction peak between (100) and (200) peaks was made by the EBSA doping in the out-of-plane (OOP) direction (Figure 8b left). In addition, this new peak seems to be more pronounced as the EBSA doping ratio increased. However, no noticeable change was observed in the in-plane (IP) direction

dx.doi.org/10.1021/am300141m | ACS Appl. Mater. Interfaces 2012, 4, 1281−1288

(Figure 8b right). On the basis of this result, we can deduce that the EBSA doping influenced the P3HT stacking in the OOP direction so that some portions of P3HT chains linked to the doped parts underwent rearrangement leading to a smaller interchain distance in the OOP direction (note that the new peak was found at a wider angle compared to the (100) peak).[22] Here it is noteworthy that this rearrangement was not so significant because similar new peak was not measured in the IP direction, which can be supported by the HRTEM result that the average *d*-spacing in the IP direction was almost not changed (see Figure S5 in the Supporting Information).

To understand the surface morphology of films after the EBSA doping, we measured the AFM images of the same samples as for the GIXD measurement. As shown in Figure 9a,

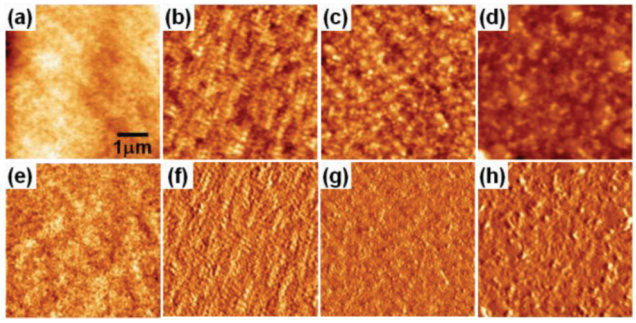

Figure 9. AFM images (scan size: 5 × 5 μm; (a–d) height mode, (e–h) phase mode) of (a, e) the PVP-MMF layer coated on the ITO-glass substrate and (b, f) the pristine P3HT layer or the P3HT-EBSA layer coated on the PVP-MMF-coated samples ((c, g) EBSA = 0.5 wt %, (d, h) EBSA = 1.0 wt %). rms roughness = (a) 0.38, (b) 1.14, (c) 3.22, and (d) 3.06 nm.

the surface of the PVP-MMF layer was extremely smooth (rms roughness = 0.38 nm). Relatively, however, the surface roughness of the pristine P3HT layer was much rougher (roughness = 1.14 nm), which can be attributed to the polycrystalline nature of the present P3HT film (see the random ripple-like domain structure in Figure 9b). Interestingly, the polycrystalline domain structure became less pronounced for the P3HT-EBSA (0.5 wt %) layer (Figure 9c). When the EBSA ratio was increased up to 1.0 wt %, the crystalline feature nearly disappeared but particle-like domains appeared (Figure 9d). However, the surface roughness was almost tripled for the doped P3HT layers. As also observed from the phase images in Figure 9f–h, this huge change in the surface morphology of P3HT films by the small amount of the dopant (EBSA) molecules can be related to the generation of new GIXD diffraction peak in Figure 8. However, we need more detailed investigation in order to directly correlate the morphology change with the OFET characteristics.

Regioregularity and Optimized Performance. Finally, we investigated the correlation between the P3HT regioregularity (RR) and the EBSA doping. As shown in Figure 10a, the maximum current at the same voltage condition was similar for RR = 92% and RR = 95%, whereas it was almost 10 times higher for RR = 98%. After the EBSA (1.0 wt %) doping, the maximum current at the same voltage condition was greatly increased irrespective of the regioregularity (Figure 10b). Interestingly, the extent of the maximum current increment by the EBSA doping was about 100 times for RR = 98% compared to 180 times for RR = 92% and 260 times for RR = 95%. This different improvement by the EBSA doping is not clear at the

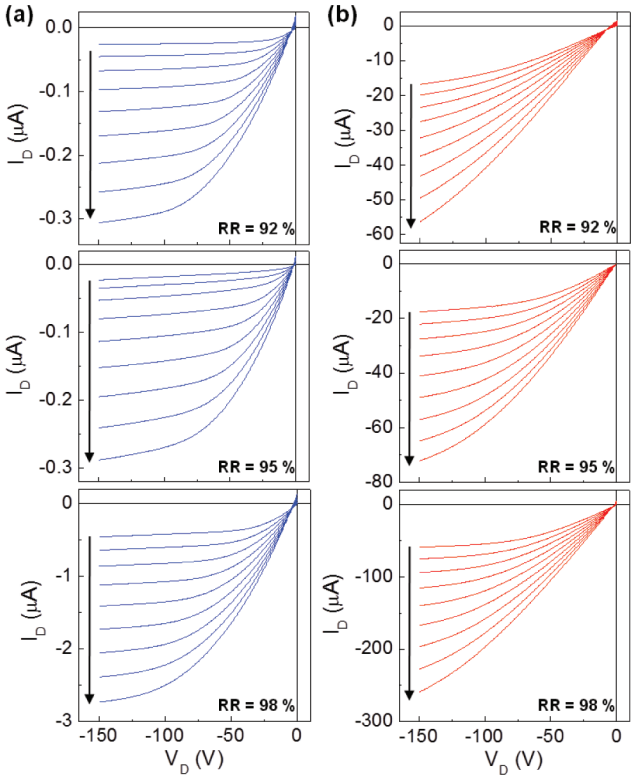

Figure 10. Effect of P3HT regioregularity (RR) on the output curves of OFETs: (a) the pristine P3HT layer, (b) the P3HT-EBSA layer. The gate voltage (V_G) increased negatively from 0 to −80 V by 10 V gap in the direction of the arrows.

moment, but the doped states are considered to be affected by the recrystallization (self-assembly) behavior because of the different portion of regiorandom and regioregular units.

As a result, the hole mobility was greatly improved by the factor of 80-fold, 86-fold, and 55-fold for 92, 95, and 98% RR P3HTs, respectively, by the EBSA doping (Figure 11). The

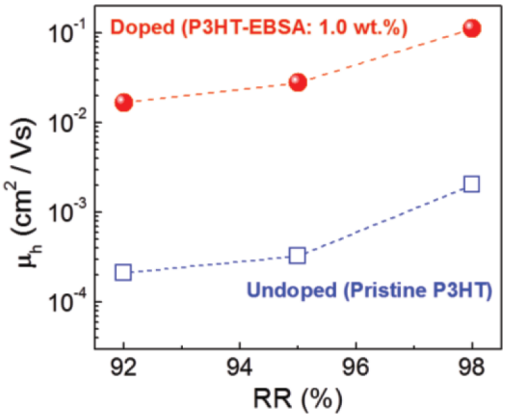

Figure 11. Hole mobility (μ_h) as a function of regioregularity (RR) for the OFETs with the pristine P3HT layer (open squares) and the P3HT-EBSA layer (filled circles).

maximum hole mobility of the 98% RR P3HT reached 0.112 cm^2/(V s) after the EBSA doping, which is one of the higher records achieved for P3HT-based OFETs even though the present OFETs employed silver metals for the source and drain electrodes, whereas gold metals were used in the previous

works.[9,24−26] However, the drain current at V_G = 0 V was still higher (leading to the poor on/off ratio), which is considered as the influence of polar hydroxyl groups that are remained (unreacted) in the PVP-MMF layer.[27,28]

To improve the on/off ratio, the precursor reaction between PVP and MMF in solutions was undertaken for sufficiently long time until the solution color changed to dark yellow (room temperature). As a consequence, the drain current at V_G = 0 V was significantly reduced from −58 to −1.8 μA for the device with the EBSA (1.0 wt %) doped P3HT (RR = 98%) layer, whereas its reduction was relatively low for the device with the pristine P3HT layer (Figure 12). In particular, the on/off ratio

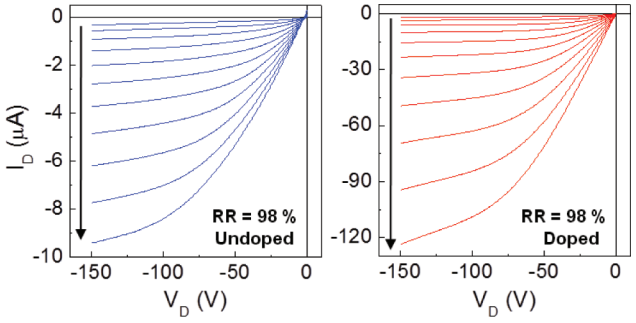

Figure 12. Output curves of OFETs with the 98% RR P3HT layers: (left) the pristine P3HT layer and (right) the P3HT-EBSA (1.0 wt %) layer. The gate voltage (V_G) increased negatively from 0 to −100 V by 10 V gap in the direction of the arrows.

was greatly improved up to 1.4 × 10^4 for the device with the P3HT-EBSA layer, though the drain current at V_G = −80 V and V_D = −150 V was decreased by ca. 1/3-fold from the value in Figure 10b. In this effort, the maximum hole mobility reached ∼0.1 cm^2/(V s) (V_G = −30 V, V_D = −150 V) for the OFET with the P3HT-EBSA layer (RR = 98% and EBSA = 1.0 wt %), whereas the OFET with the pristine P3HT layer exhibited ∼0.01 cm^2/(V s) at the same condition (see Figure S6 in the Supporting Information).

CONCLUSIONS

The P3HT polymers were doped with EBSA molecules to improve their charge transport characteristics. A weak shoulder peak at around 970 nm (∼1.3 eV), which is related to the EBSA-doped thiophene units in the P3HT chains, was newly made by the EBSA doping (1.0 wt %), whereas the PL intensity was noticeably reduced by only 1.0 wt % EBSA doping. The evidence for the EBSA-doped thiophene units were measured from the S2p XPS spectra that were shifted toward higher energy regions as the EBSA content increased. In addition, we also found that the HOMO energy level was marginally shifted toward lower energy regions as the EBSA content increased. Based on the analyzed results, we proposed the mixed-band charge transport mechanism, which features the mixed hole-transporting energy bands (paths) created by both field-effect and EBSA doping, leading to the improved hole mobility. As expected from the proposed mechanism, the drain current of OFETs with the P3HT-EBSA layer (RR = 92%) was significantly increased as the EBSA content increased, whereas the hole mobility was slowly increased at lower EBSA contents and the increment became bigger at higher EBSA contents. In terms of nanostructure changes, new diffraction peak at around (100) peaks in the OOP direction was measured for the doped P3HT layers, whereas the surface nanomorphology was noticeably changed with the EBSA content. The present doping effect was similarly observed for the P3HTs with different regioregularities. The hole mobility after the EBSA doping was increased by the factor of 55−86 depending on the regioregularity in the case of using the (imperfect) PVP-MMF layer with many unreacted hydroxyl groups, while the OFET with the optimized PVP-MMF layer exhibited ∼10 times increased hole mobility by the 1.0 wt % EBSA doping compared to the device with the pristine P3HT layer. Hence the present partial doping method is expected to be effectively applied for other types of semiconducting polymers so that it could contribute to the improved performance of organic electronic devices such as polymer solar cells, organic memory devices, organic phototransistors, etc.[29−31]

ASSOCIATED CONTENT

Supporting Information

Optical absorption spectra, output and transfer curves for the unannealed OFETs with the P3HT-EBSA layers (whole doping ratios), output and transfer curves for the annealed OFETs, hole mobility comparison between unannealed and annealed OFETs according to the EBSA doping ratios, and HRTEM images of the pristine P3HT film and the P3HT-EBSA film (PDF). This material is available free of charge via the Internet at http://pubs.acs.org.

AUTHOR INFORMATION

Corresponding Author

*Phone: +82 53 950 5616. E-mail: ykimm@knu.ac.kr; khj217@knu.ac.kr; csha@pusan.ac.kr.

Notes

The authors declare no competing financial interest.

ACKNOWLEDGMENTS

This work was financially supported by Korean Government grants (Basic Research Laboratory Program_2011-0020264, Pioneer Research Center Program_2011-0001646 and 2011-0001667/0001668, Priority Research Center Program_2009-0093819, Acceleration Research Program_2011-0000385, NRF_2009-0072777, NRF_2010-0004164, NRF_2011-0007085) and by Pohang Accelerator Laboratory for the synchrotron X-ray diffraction measurements.

REFERENCES

(1) Kudo, K.; Yamashina, M.; *Jpn. J. Appl. Phys.*, Part 1. **1984**, *23*, 130-130.
(2) Tsao, H. N.; Müllen, K. *Chem. Soc. Rev.* **2010**, *39*, 2372−2386.
(3) Ortiz, R. P.; Facchetti, A.; Marks, T. J. *Chem. Rev.* **2010**, *110*, 205−239.
(4) Rovira, C.; Mas-Torrent, M. *Chem. Rev.* **2011**, *111*, 4833−4856.
(5) Guo, Y.; Yu, G.; Liu, Y. *Adv. Mater.* **2010**, *22*, 4427−4447.
(6) Park, S. K.; Jackson, T. N.; Anthony, J. E.; Mourey, D. A. *Appl. Phys. Lett.* **2007**, *91*, 063514.
(7) Sundar, V. C.; Zaumseil, J.; Podzorov, V.; Menard, E.; Willett, R. L.; Someya, T.; Gershenson, M. E.; Rogers, J. A. *Science* **2004**, *303*, 1644−1646.
(8) Taso, H. N.; Cho, D. M.; Park, I.; Hansen, M. R.; Mavrinskiy, A.; Yoon, D. Y.; Graf, Robert.; Pisula, W.; Spiess, H. W.; Müllen, K. *J. Am. Chem. Soc.* **2011**, *133*, 2605−2612.
(9) Sirringhaus, H.; Brown, P. J.; Friend, R. H.; Nielsen, M. M.; Bechgaard, K.; Langeveld-Voss, B. M. W.; Spiering, A. J. H.; Janssen, R. A. J.; Meijer, E. W.; Herwig, P.; de Leeuw, D. M. *Nature* **1999**, *401*, 685−688.

(10) Kim, Y.; Cook, S.; Tuladhar, S. M.; Choulis, S. A.; Nelson, J.; Durrant, J. R.; Bradley, D. D. C.; Giles, M.; McCulloch, I.; Ha, C. S.; Ree, M. *Nat. Mater.* **2006**, *5*, 197−203.
(11) Arkhipov, V. I.; Heremans, P.; Emelianova, E. V.; Adriaenssens, G. J.; Bassler, H. *Appl. Phys. Lett.* **2003**, *82*, 3245−3247.
(12) Abe, Y.; Hasegawa, T.; Takahashi, Y.; Yamada, T.; Tokura, T. *Appl. Phys. Lett.* **2005**, *87*, 153506.
(13) Lim, E.; Jung, B. J.; Chikamatsu, M.; Azumi, R.; Yoshida, Y.; Yase, K.; Do, L. M.; Shim, H. K. *J. Mater Chem.* **2007**, *17*, 1416−1420.
(14) Ma, L.; Lee, W. H.; Park, Y. D.; Kim, J. S.; Lee, H. S.; Cho, K. *Appl. Phys. Lett.* **2008**, *92*, 063310.
(15) Nam, S.; Lee, S.; Lee, I.; Shin, M.; Kim, H.; Kim, Y. *Nanoscale* **2011**, *3*, 4261−4269.
(16) Kanemoto, K.; Shishido, M.; Sudo, T.; Akai, I.; Karasawa, T.; Agari, Y *Synth. Met.* **2005**, *155*, 162−167.
(17) Kanemoto, K.; Shishido, M.; Sudo, T.; Akai, I; Hashimoto, H.; Karasawa, T. *Chem. Phys. Lett.* **2005**, *402*, 549−553.
(18) Kim, H.; Nam, S.; Lee, H.; Woo, S.; Ha, C. S.; Ree, M.; Kim, Y. *J. Phys. Chem. C.* **2011**, *115*, 13502−13510.
(19) Fung, M. K.; Lai, S. L.; Tong, S. W.; Bao, S. N.; Lee, C. S.; Wu, W. W.; Inbasekaran, M.; O'brien, J. J.; Lee, S. T. *J. Appl. Phys.* **2003**, *94*, 5763−5770.
(20) Nam, S.; Shin, M.; Kim, H.; Ha, C. S.; Ree, M.; Kim, Y. *Adv. Funct. Mater.* **2011**, *21*, 4527−4534.
(21) Kim, H.; Shin, M.; Kim, Y. *Macromol.Res.* **2009**, *17*, 445−447.
(22) Shin, M.; Kim, H.; Park, J.; Nam, S.; Heo, K.; Ree, M.; Ha, C. S.; Kim, Y. *Adv. Funct. Mater.* **2010**, *20*, 748−754.
(23) Nam, S.; Shin, M.; Kim, H.; Kim, Y. *Nanoscale* **2010**, *2*, 2384−2389.
(24) Wang, G.; Swensen, J.; Moses, D.; Heeger, A. J. *J. Appl. Phys.* **2003**, *93*, 6137−6141.
(25) Park, J.; Park, S. Y.; Shim, S. O.; Kang, H.; Lee, H. H. *Appl. Phys. Lett.* **2004**, *85*, 3283−3285.
(26) Cho, J. H.; Lee, J.; Xia, Y.; Kim, B.; He, Y.; Renn, M. J.; Lodge, T. P.; Frisbie, C. D. *Nat. Mater.* **2008**, *7*, 900−906.
(27) Lim, S. C.; Kim, S. H.; Koo, J. B.; Lee, J. H.; Ku, C. H.; Yang, Y. S.; Zyung, T. *Appl. Phys. Lett.* **2007**, *90*, 173512.
(28) Kim, S. J.; Lee, J. S. *Nano Lett.* **2010**, *10*, 2884−2890.
(29) Shin, M.; Kim, H.; Kim, Y. *Macromol.Res.* **2010**, *18*, 709−712.
(30) Gupta, R. K.; Kusuma, D. Y.; Lee, P. S.; Srinivasan, M. P. *ACS Appl. Mater. Interfaces* **2011**, *3*, 4619−2635 and references therein.
(31) Hwang, H.; Kim, H.; Nam, S.; Bradley, D. D. C.; Kim, Y. *Nanoscale* **2011**, *3*, 2275−2279.